SLOWLY MOVING BLACK HOLES IN KHRONO-METRIC MODEL

SLOWLY MOVING BLACK HOLES IN KHRONO-METRIC MODEL

By ANDREW JAMES KOVACHIK, BS

A Thesis Submitted to the School of Graduate Studies in Partial Fulfillment of the Requirements for the Degree Master of Science

McMaster University

MASTER OF SCIENCE (2022)

Hamilton, Ontario, Canada (Physics and Astronomy)

TITLE:	Slowly Moving Black Holes in Khrono-Metric Model
AUTHOR:	Andrew James Kovachik BS (Physics and Astronomy), University of Waterloo, Waterloo, Canada
SUPERVISOR:	Sergey Sibiryakov
NUMBER OF PAGES:	xii, 53

Lay Abstract

I have investigated slowly moving black holes in a theory of modified gravity. The goal was to see whether the theory breaks down in modelling these black holes and if not, is it possible to test the theory using these predictions. I ultimately found that this theory can model the slowly moving black holes and would appear almost indistinguishable from classically moving black holes. This means that slowly moving black holes on their own will not provide a sufficient test of the theory.

Abstract

I have developed a technique to solve for the khronon field in a space-time containing a slowly moving black hole in the khrono-metric regime of Hořava Gravity. To develop these solutions I first revisited the khronon field around static spherically symmetric black holes and perturbed them by a small velocity. The equations of motions of the perturbed field were identified along with the linearly dependent series expansions at the boundary points. Using the boundary conditions and equations of motion the khronon field was numerically solved throughout the space-time. These solutions were used to calculate a sensitivity parameter which defines how the black hole mass appears to be modified due to its velocity. It was found that the sensitivity parameters are highly suppressed and black holes should appear similar to their general relativity counterpart.

To my family, my teachers, and to Paige.

For your endless support

Acknowledgements

I would like to express my gratitude to several individuals who have played an enormous role in the completion of this thesis. First and foremost, I extend my greatest appreciation to my supervisor, Sergey. Your patience, guidance, and the invaluable time you invested in teaching me over the past two years have been instrumental in shaping the outcome of this work. I am also deeply thankful to Jury, who not only served as a mentor throughout my university proceedings but became a true friend. Your support and encouragement have been indispensable. As well, I also extend my appreciation to Cliff, Duncan, and Sung-Sik for their time and knowledge during my Committee meeting and defence.

I owe a debt of gratitude to my friend and former colleague, Basel. Your willingness to engage in discussions late into the night to share ideas and insights has greatly enriched my research. I would also like to acknowledge McMaster University for providing me with the opportunity to study here and in cooperation with the Government of Ontario for awarding me the Ontario Graduate Scholarship (OGS). This support has saved me from the financial burden of my education and research.

Last, I want to thank Paige for her unwavering support and ability to keep me calm during challenging times. Your endless encouragement will never go unappreciated and I will strive to repay it tenfold in any task you set out to accomplish.

Table of Contents

Lay Abstract **iii**

Abstract **iv**

Acknowledgements **vi**

Notation, Definitions, and Abbreviations **xi**

Declaration of Academic Achievement **xiii**

1 Introduction **1**

2 Analysis **4**

2.1 Khrono-Metric Model 4

2.2 Background Solution 8

2.3 Moving Black Hole 14

2.4 Sensitivities 32

3 Results **40**

A Additional Calculations **42**

A.1 Stress Energy Deviation 42
A.2 Metric Perturbation corrections 45

B Additional Figures **46**

B.1 Additional Figures 46

List of Figures

1 Hořava gravity foliations 5

2 Background field solutions 12

3 Moving black hole frames of reference 16

4 Perturbed field solutions 29

5 Example Aether Perturbation 30

6 χ_0 parameter fit 38

7 Background field high derivatives 47

8 Numerical functions for small khronon speed 48

9 Numerical functions for large khronon speed 49

10 Non divergent perturbed field solutions 49

List of Tables

1 A, B, and C order of roots 19

2 Minimally allowed powers series expansion of khronon field 21

3 Linearly independent perturbation solutions 24

4 Infinite sound speed perturbation orders 32

5 χ_0 list 39

Notation, Definitions, and Abbreviations

Notation

$\sqrt{-g}$	Covariant volume element

Definitions

sig(g)	$(+,-,-,-)$

Khronon field

Field which describes the foliation of time

Decoupling limit

Regime where the coupling parameters of the theory are small compared to curvature so that the back reaction of the khronon field onto the metric may be ignored

Shooting method

Iterative approach to solving a differential equation with boundary

conditions at two or more different points

Abbreviations

GR	General relativitiy
HG	Horava gravity
AE	Einstein Aether gravity
QG	Quantum gravity

Declaration of Academic Achievement

I certify that the work presented in this thesis is my own completed over the period of my Master's degree at McMaster University.

Chapter 1

Introduction

The common issue with attempting to quantize general relativity (GR) is that one finds that to ensure renormalizability the theory requires terms of order $1/p^4$. These factors lead to frequency terms of order $p^4 = (\omega^2 - k^2)^2 = \mathcal{O}(\omega)^4$, which will imply that the wave equations of the theory will be fourth order in time $\mathcal{O}(\omega)^4 \implies \ddddot{\psi}$. These higher time derivatives cause small fluctuations to have negative energy and destabilize the vacuum, a scenario that contradicts our macroscopic observations, where small quantum fluctuations don't seem to give rise to large-scale variations.

In an attempt to develop a quantum theory of gravity (QG), Petr Hořava proposed a model in 2009 [1] that allow for anisotropic scaling between space and time. This anisotropic scaling takes the form of $t \to b^{-z}t,\ x \to b^{-1}x$.

For a scaling exponent z large enough the theory is power-counting renormalizable. However, this modification creates changes to the large-scale, gravitational, structure of the theory. Most notably, the theory breaks Lorentz invariance (LI), which allows for the propagation of signals faster than light. Deviations from LI will mostly occur at the highest energies, but also affects low-energy gravitational physics.

The anisotropic scaling present in Hořava gravity will cause the propagation of signals to be dependent on foliations of a scalar field, known as the khronon field. The physical observable of this field is its normalized gradient, which depicts the preferred time direction. This ensures that the khronon field is invariant under relabeling, $\phi_{\text{kh}} \to f(\phi_{\text{kh}})$. To lowest order, the khronon gradient enters the classic GR action at second order.

Massive celestial bodies such as pulsars or black holes are natural subjects for investigating these changes, and they have yielded numerous intriguing results. For instance, at high energies, there can be infinitely fast propagation of modes. Yet, it was discovered that black holes in the theory possess a universal horizon that entraps even these superluminal modes [2]. Consequently, two causally disconnected regions still persist.

Previous studies have uncovered khronon solutions for stationary black holes [3] and rotating black holes [4]. However, a phenomenology of these solutions is required to test the theory. For this need, we will turn to sensitivity parameters [5] which characterize the dependence of a black hole's mass on its velocity. Sensitivity parameters have been regularly calculated in Einstein-Aether (AE) theory [6–9], a theory related to HG. In this thesis, we will expand these findings by investigating and deriving a set of solutions for moving black holes. These solutions will then be used to calculate a sensitivity parameter to identify the theoretical regimes potentially accessible by future gravitational wave experiments [10, 11].

While earlier work [12] has determined sensitivities for a specific choice of HG model parameters, the paper suggested that a general set of solutions might be impossible. In this thesis we show that a general set of solutions can be found. To

simplify the problem, we work in the limit where the khronon energy-momentum tensor is small compared to the GR curvature term, known as the *decoupling limit*. We will use the decoupling limit to determine the khronon field in a classical GR solution, in our case we find solutions on a Schwarzschild black hole background. We will begin by determining the field for stationary black holes and subsequently introduce a perturbation to the background solution in terms of the small velocity. In the perturbation limit the correction to the khronon field will then be solved. Lastly, we will identify an observable of the theory known as a sensitivity parameter. We will find that this parameter is strongly suppressed indicating that slowly moving black holes behave like their GR counterpart.

Chapter 2

Analysis

2.1 Khrono-Metric Model

The nature of breaking Lorentz invariance can be thought of as creating a foliation in space-time. The gradient of this foliation defines the preferred flow of time. In general relativity, this foliation would be viewed as spacelike surfaces, so that the preferred flow is in the time direction Figure.1a. In Hořava gravity where space and time are no longer on equal footing one can imagine the foliations as bending and flexing so that the preferred time direction is no longer purely in the time coordinate direction Figure.1b.

The foliation is described by the field ϕ, the khronon scalar field. We define a vector u_μ so that it points along the preferred time direction[1]:

$$u_\mu \equiv \frac{\partial_\mu \phi}{\sqrt{\partial_\nu \phi \partial^\nu \phi}}. \tag{2.1.1}$$

[1]We use the metric signature $(+,-,-,-)$.

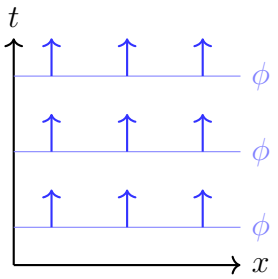

(a) Preferred time foliation

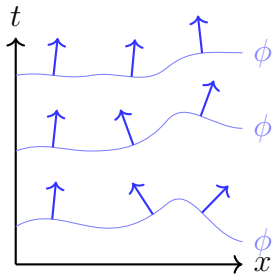

(b) Khronon field with perturbation

Figure 1: Hořava gravity foliations: Khronon field with and without perturbations.

This vector, which we will refer to as aether, is invariant under the re-parametrization of the khronon $\phi \to f(\phi)$, which is imposed as the symmetry of the model. This implementation is very similar to that of Einstein-Aether theory which involves just the implementation of a unit norm vector field but does not require it to be derived from some scalar field as we have done above. If we add the khronon to the classical action for general relativity at the lowest order in derivatives we get:

$$S = \frac{-M^2}{2}\int \mathrm{d}^4x\sqrt{-g}\Big(R + \alpha(u^\mu\nabla_\mu u_\nu)^2 + \beta(\nabla_\mu u^\nu)(\nabla_\nu u^\mu) + \lambda(\nabla_\mu u^\mu)^2\Big) \tag{2.1.2}$$

One might question why the lowest order terms don't contain the vector u^μ without derivatives. This is because the vector u^μ was constructed in such a way that its norm $u^\mu u_\mu = 1$. As a result, any terms that contain different orders of u_μ without derivatives produce a constant, which can be ignored in the action.

From this point, we wish to simplify the action and metric to aid in analyzing the physics of the problem. The first step is to consider the limit where the coupling parameters are small, $\alpha, \beta, \lambda \ll 1$. In this limit, the Einstein field equations will have a contribution by the khronon field of $T^{(\phi)}_{\mu,\nu}$ scaled by factors of α, β, λ. Since these

coupling parameters are small the Einstein field equation, to leading order, looks like what is obtained in standard general relativity. We are then able to choose the metric to be those found in general relativity and to leading order ignore the back reaction of the khronon field on the metric. This limit is referred to as the *decoupling limit* of the theory.

In the decoupling limit of the theory we will choose to solve the khronon field in the Schwarzschild metric which has the form of:

$$\mathrm{d}s^2 = \left(1 - \frac{1}{r}\right)\mathrm{d}t^2 - \left(1 - \frac{1}{r}\right)^{-1}\mathrm{d}r^2 - r^2\,\mathrm{d}\Omega^2\,, \tag{2.1.3}$$

where we have chosen to set the Schwarzschild radius, $r_s = 2GM = 1$ and $\mathrm{d}\Omega^2$ is the metric on a unit 2-sphere. For the metric to be non-singular at the Schwarzschild radius we convert to Eddington-Finkelstein coordinates with $v = t + r + \log(r-1)$ so that the metric takes the form:

$$\mathrm{d}s^2 = \left(1 - \frac{1}{r}\right)\mathrm{d}v^2 - 2\,\mathrm{d}r\,\mathrm{d}v - r^2\,\mathrm{d}\Omega^2\,. \tag{2.1.4}$$

Lastly, it will be convenient to work in coordinates with inverse radius, $\xi = 1/r$, which gives the final form of the metric as:

$$\mathrm{d}s^2 = (1-\xi)\,\mathrm{d}v^2 + \frac{2}{\xi^2}\,\mathrm{d}\xi\,\mathrm{d}v - \frac{1}{\xi^2}\,\mathrm{d}\Omega^2 \tag{2.1.5}$$

Now, we will simplify the action of the khronon field to reduce the number of

terms. First, we introduce the following definitions:

$$u_{\mu\nu} \equiv \partial_\mu u_\nu - \partial_\nu u_\mu \tag{2.1.6}$$

$$c_\chi = \sqrt{\frac{\beta + \lambda}{\alpha}}, \tag{2.1.7}$$

Then, the curl of the khronon vector field should be zero as it is a hypersurface orthogonal vector:

$$\text{Curl}(u) = w_\mu = \epsilon_{\mu\nu\rho\sigma} u^\nu \nabla^\rho u^\sigma = 0. \tag{2.1.8}$$

Using this, consider the inner product of the vector w^μ with itself:

$$w_\mu w^\mu = (\epsilon^{\mu\nu'\rho'\sigma'} u_{\nu'} \nabla_{\rho'} u_{\sigma'})(\epsilon_{\mu\nu\rho\sigma} u^\nu \nabla^\rho u^\sigma) = (u^\nu \nabla_\nu u_\mu)^2 - \frac{1}{2} u_{\mu\nu} u^{\mu\nu} = 0. \tag{2.1.9}$$

Equation (2.1.9) implies:

$$(u^\nu \nabla_\nu u_\mu)^2 = \frac{1}{2} u_{\mu\nu} u^{\mu\nu}. \tag{2.1.10}$$

Equation (2.1.10) is used to replace the term with the coefficient α. The term with coefficient β is re-written by integrating by parts the covariant derivative, commuting the two covariant derivatives, and integrating by parts again:

$$\beta \int \mathrm{d}^4x \sqrt{-g} \boldsymbol{\nabla}_\mu u^\nu \boldsymbol{\nabla}_\nu u^\mu = \beta \int \mathrm{d}^4x \sqrt{-g} (\boldsymbol{\nabla}_\nu u^\nu)^2 - R_{\mu\nu} u^\mu u^\nu. \tag{2.1.11}$$

In the Schwarzschild metric the Ricci tensor is zero, allowing us to combine the λ, β terms to re-write the khronon contribution to the action as:

$$S_\phi = -\alpha M^2 \int \mathrm{d}^4x \sqrt{-g} \left(\frac{1}{4} u_{\mu\nu} u^{\mu\nu} + \frac{c_\chi^2}{2} (\boldsymbol{\nabla}_\mu u^\mu)^2 \right). \tag{2.1.12}$$

The coefficient c_χ describes the speed of the khronon modes and is colloquially referred to as the "*sound speed*" of the khronon field.

2.2 Background Solution

2.2.1 Khronon with Stationary Black Hole

In this section we find solutions for the khronon field in the presence of a static black hole following the approach of [3]. To do so, we derive the equations of motion from the khronon action, identify the boundary conditions, and numerically solve the equations of motion to obtain solutions for the khronon.

Starting from the action for the khronon field as given in (2.1.12), we find its variation with respect to the khronon field. First note:

$$\delta u_\mu = \frac{1}{\sqrt{X}}(\nabla_\nu \delta\phi - u_\nu u_\mu \nabla^\mu \delta\phi), \tag{2.2.1}$$

where $X = \nabla_\mu \phi \nabla^\mu \phi$. The variation of the Lagrangian after integration by parts and requiring that the variation at the boundary goes to zero gives:

$$\delta\mathcal{L} \approx \frac{\delta S_\phi}{\delta u_\nu}\delta u_\nu. \tag{2.2.2}$$

Inserting the variation of the vector field and integrating by parts gives:

$$\delta\mathcal{L} \approx \left[\nabla_\lambda \left(\frac{\delta^\lambda_\nu - u^\lambda u_\nu}{\sqrt{X}}\frac{\delta S_\phi}{\delta u_\nu}\right)\right]\delta\phi. \tag{2.2.3}$$

Therefore, we can write the equations of motion for the khronon field as a current

conservation:

$$\nabla_\lambda J^\lambda = 0, \tag{2.2.4}$$

where:

$$J^\lambda = \frac{\delta^\lambda_\nu - u^\lambda u_\nu}{\sqrt{X}} \frac{\delta S_\phi}{\delta u_\nu}. \tag{2.2.5}$$

Next, we notice two things. Firstly, we can expand (2.2.4) in Schwarzschild coordinates to get:

$$\partial_t J^t + \partial_r J^r = -\frac{2J^r}{r} \tag{2.2.6}$$

where we make use of the spherical symmetry of the problem to get $J^\theta = J^\phi = 0$. Since the field is static, we also have that $J^t = 0$. Treating the component of J^r as an independent variable we can integrate (2.2.6) to get:

$$J^r = \frac{C_1}{r^2}. \tag{2.2.7}$$

Secondly, we expand the explicit form of J^r from the exact form derived in (2.2.5) to get:

$$J^r = \frac{1}{\sqrt{X}} \left[u^r u_t \left(\partial_r^2 u_t + \frac{2}{r} \partial_r u_t \right) - c_\chi^2 u_t^2 \partial_r \left(\partial_r u^r + \frac{2}{r} u^r \right) \right] \tag{2.2.8}$$

we can then equate both (2.2.7) and (2.2.8). Using the fact that u should have a unit norm we can write:

$$u_t^2 = (u^r)^2 - \frac{1}{r} + 1 = (u^r)^2 - \xi + 1 \tag{2.2.9}$$

to replace u_t in terms of u^r. The upper and lower indices of u_t and u^r were chosen so that in Eddington-Finkelstein coordinates the coordinates remain regular and coincide

with the Schwarzschild coordinates:

$$u_t|_{\text{Sch}} = u_v|_{\text{EF}}, \quad u^r|_{\text{Sch}} = u^r|_{\text{EF}} \tag{2.2.10}$$

Then, by considering the field at large radius we compare the left and right hand side of the equation and identify that u^r has the form of:

$$u^r = \frac{C_1}{2c_\chi^2} + \frac{C_2}{r^2} + C_3 r. \tag{2.2.11}$$

If we enforce that the radial component of the aether vanishes at infinity we get that $C_1 = C_3 = 0$ and we can then see that J^r in fact satisfies a stronger condition $J^r = 0$. Lastly, we will introduce the notation:

$$U \equiv u_t, \quad V \equiv u^r \tag{2.2.12}$$

which allows us to write the equations of motion in a compact form:

$$\frac{U''}{U} - c_\chi^2 \left(\frac{V''}{V} + \frac{2}{\xi^2} \right) = 0, \tag{2.2.13}$$

where primes denote differentiation with respect to ξ. After substituting V for U using the unit norm (2.2.9) gives:

$$U'' = -\frac{c_\chi^2 U}{U^2(1-c_\chi^2) - 1 + \xi} \left[-(U')^2 + \frac{(UU' + \frac{1}{2})^2}{U^2 - 1 + \xi} + \frac{2(U^2 - 1 + \xi)}{\xi^2} \right] \tag{2.2.14}$$

Let us now consider the boundary conditions for the function U. At spatial infinity the effect of the black hole should become negligible, causing the vector field to look

like it is purely time-like, $u^\mu = (1, 0, 0, 0)$. In our new notation, we are expecting the vector to be purely time-pointing, or $U(\xi = 0) = 1$. Since we wish to find solutions that are stationary and spherically symmetric the above condition tells us that ϕ should have no dependence on θ or ϕ, and only change with r and go to t at spatial infinity. Putting these conditions together we get that ϕ will have the form of:

$$\bar{\phi} = t + f(r) \tag{2.2.15}$$

where $f(r) \to 0$ as $r \to \infty$

Lastly, return to the equation of motion (2.2.14), the differential equation has two singularities, one at $\xi = 0$, and another at $\xi = \xi_c$ defined by:

$$(1 - c_\chi^2)U^2(\xi_c) = 1 - \xi_c. \tag{2.2.16}$$

This point represents the horizon for khronon perturbations, or the "*sound horizon*". Requiring the solution to be regular at these two singular points supplies us with the additional boundary conditions. For instance at ξ_c the term inside of the square brackets in (2.2.14) must vanish. This constraint defines the form of $U'(\xi_c)$:

$$U'(\xi_c) = \frac{1}{2}\left(-\frac{1}{1-\xi_c}\sqrt{\frac{1-\xi_c}{1-c_\chi^2}} \pm \sqrt{\frac{c_\chi^4(8 + \xi_c(9\xi_c - 16)) - c_\chi^2\xi_c^2}{(1-c_\chi^2)^2(\xi_c - 1)\xi_c^2}}\right) \tag{2.2.17}$$

The negative sign is chosen so that the expression is well defined for $c_\chi \to 1$. Suppression of the singularity at $\xi = 0$ is then used as a condition in the numerical procedure to obtain the correct solution of U. We now move to solving this differential equation numerically.

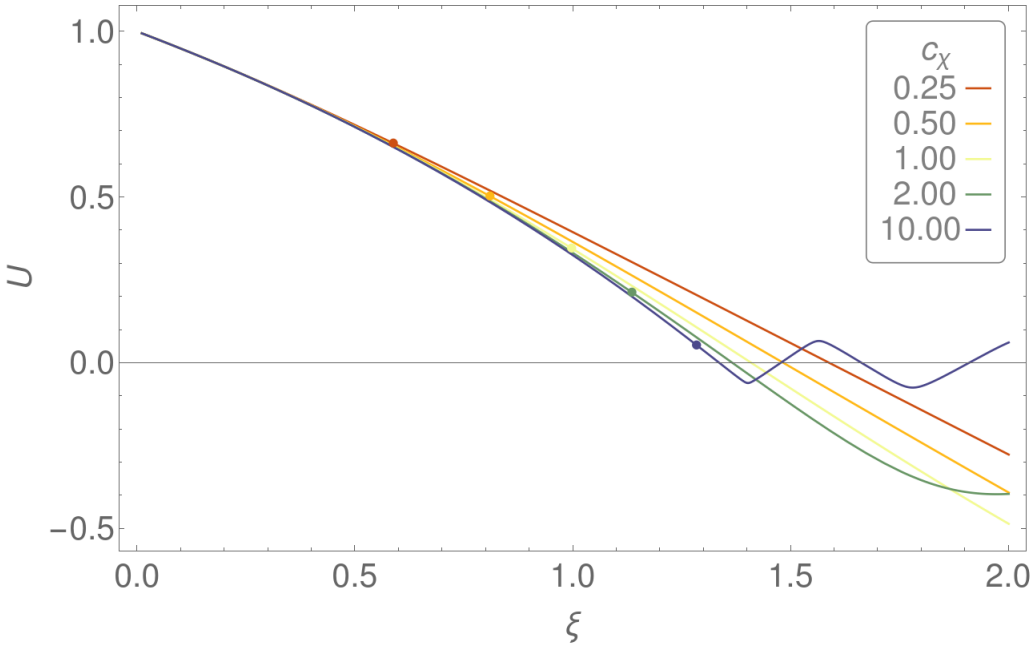

Figure 2: Background field solutions
Solutions of U for different values of c_χ. The colored points represent the position of the sound horizon for the corresponding colored line. The points where the curve first crosses zero mark the position of the universal horizon $\xi_\star$. Note that $\xi_\star$ and ξ_c both approach 4/3, as $c_\chi \to \infty$.

2.2.2 Stationary Black Hole Solution

We now wish to find numerical solutions to the equation of motion for the khronon field that satisfies the boundary conditions described above. We have the freedom to choose which point to begin solving the differential equation. In this thesis, we choose the point ξ_c so as to easily enforce a non-singular behaviour. However, for a given c_χ the value of $U(\xi_c)$ depends on ξ_c which is not known ahead of time. To account for this in an iterative manner a value of ξ_c is guessed which defines $U(\xi_c)$, and $U'(\xi_c)$ and the differential equation is solved towards $\xi = 0$. This solution is checked to see if it satisfies the boundary condition at the origin and based on how well the condition is satisfied a new value of ξ_c is guessed. The process of making better guesses of ξ_c

to satisfy a boundary condition at another point is called a "*shooting method*". The process is repeated until a satisfactory precision is reached.

In practice, there are some minor complications that need to be considered during the shooting method. First, because of the singularity at ξ_c, shooting from this point, even with defining $U(\xi_c)$ to be finite the solution may diverge immediately due to numerical inaccuracies. To account for this divergence the shooting method is actually done at a point $U(\xi_c - \epsilon)$ as an initial condition. Secondly, the solution at $\xi = 0$ is very sensitive to the initial guess and so the function generally diverges outside of numerical precision before reaching a distance of ϵ. The approach to dealing with this divergence was to use a nested iterative approach; the solution solved backward from the point $U(\xi_c)$ was matched with the $\xi = 0$ boundary condition evaluated at point $\epsilon = 0.1$ away. Then, using this final result as an initial guess the value of ϵ was decreased until it reached a sufficient minimal size (for example matching at each step of $[0.1, 0.09, 0.08, \cdots, 0.01]$). Once a solution is found that sufficiently satisfies the boundary condition towards spatial infinity ($\xi = 0$). The solution was analytically continued by Taylor expansion to the point $\xi_c + \epsilon$ and the differential equation was also solved for $\xi > \xi_c$.

We now have sufficient solutions for the spherically symmetric static black holes and their results are shown in Figure.2. Notice that each solution of Figure.2 crosses through 0. This point is often called the universal horizon and labelled $\xi_\star$. It is critical as at this point the foliation sheets become sheets of constant radius, and so the preferred time direction points inwards to the black hole. The point was critical to realizing black hole singularities in Khrono-metric theory still remain hidden despite the infinite speeds allowed.

2.3 Moving Black Hole

Now having solutions for the static spherically symmetric black holes we can move to creating a set of solutions of slowly moving black holes. To create moving black hole solutions, we will take the khronon solutions from the static black holes and add a perturbation:

$$\phi = \bar{\phi} + \mathrm{v}\ \Xi(r, \theta, \varphi). \tag{2.3.1}$$

Where the perturbation parameter is in terms of v. To solve for Ξ we will move to the frame where the black hole is static and the khronon field is tilted. We will use this frame to determine the form of the tilt at spatial infinity. Then, after deriving the equations of motion that describe the perturbed khronon field we will identify a number of points that have singular behaviour. At these points we will enforce that the normalized khronon field gradient (2.1.1) remains continuous and finite which will provide a number of constraints on the allowed solutions. We will verify that the number of constraints is just enough to uniquely define the solution. Numerical methods will then be employed to solve the khronon field.

2.3.1 Boundary Conditions at Infinity

We now seek to determine the boundary condition for the perturbation of the scalar field in the case of a slowly moving black hole. Consider first the case of a moving black hole in the frame of the khronon. In this view, at spatial infinity, the vector field should still look like $u^\mu = (1, 0, 0, 0)$. However, it is easier to view the setup from the perspective of the black hole being at rest with the khronon field being tilted in the direction opposite to that of the velocity. Now, at spatial infinity, there will

be a radial component to the vector u^μ proportional to the velocity and the angle made with the direction of the velocity. For an intuitive picture of this tilt consider Figure.3.

Given the symmetries of the problem, it is natural to assume that the solution can be decomposed into a radial function and an angular function. The angular function is decomposed into spherical harmonics:

$$\Xi = \sum_{m,\ell} c Y_\ell^m(\theta, \varphi)\chi_{m\ell}(\xi). \tag{2.3.2}$$

The spatial components of the gradient of the khronon field at spatial infinity based on our required boundary condition have the form of:

$$u^i = -\mathrm{v}^i, \tag{2.3.3}$$

which in terms of spherical coordinates would look like:

$$u^r(r \to \infty) = -\mathrm{v}\cos(\theta). \tag{2.3.4}$$

When these forms are compared to the spherical harmonic ansatz of χ we infer that only the dipolar spherical harmonic aligns with the ansatz and that the radial component must scale like r. Thus, χ should look like:

$$\chi = vrY(\theta) = \frac{\mathrm{v}}{\xi}\cos\theta \tag{2.3.5}$$

where we have taken the configuration independent of the azimuthal angle φ. The

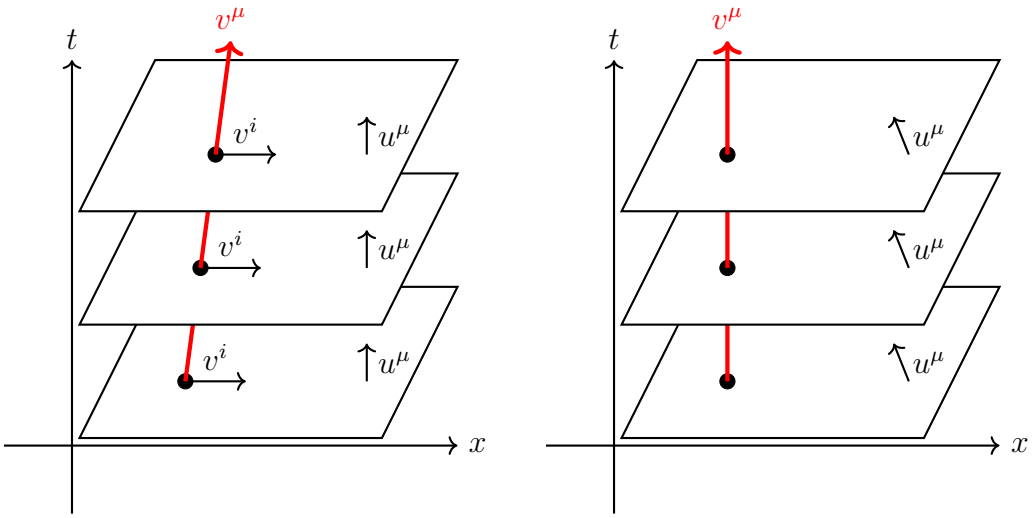

(a) Moving black hole with stationary khronon

(b) Stationary black hole with tilted khronon field

Figure 3: Moving black hole frames of reference.

2-sphere Laplacian acts on Ξ like:

$$\Delta_{S(2)}\chi = \frac{\mathrm{v}}{\xi}\Delta_{S(2)}Y_1^1 = -2\frac{\mathrm{v}}{\xi}Y_1^1 = -2\chi. \tag{2.3.6}$$

2.3.2 Equations of Motion

We now establish the equations of motions that describe the perturbation on top of the background solution. To develop these solutions, we simplify the action by aligning the time coordinate with the background khronon field:

$$\tau = \bar{\phi} = v + f(\xi). \tag{2.3.7}$$

When taking the total derivative of the new time coordinate we isolate for $\mathrm{d}v$:

$$\begin{aligned} \mathrm{d}v &= \mathrm{d}\tau - f'(\xi)\,\mathrm{d}\xi \\ \mathrm{d}v^2 &= \mathrm{d}\tau^2 + (f'(\xi))^2\,\mathrm{d}\xi^2 - 2f'(\xi)\,\mathrm{d}\xi\,\mathrm{d}\tau\,, \end{aligned} \tag{2.3.8}$$

however, we now need to identify $f'(\xi)$ in terms of U, V. To do so, notice the convenient relationship because:

$$u_\xi = \frac{\partial_\xi \bar{\phi}}{\sqrt{X}} = \frac{\partial_\xi f(\xi)}{\sqrt{X}}, \tag{2.3.9}$$

and

$$u_v = \frac{\partial_v \bar{\phi}}{\sqrt{X}} = \frac{1}{\sqrt{X}}, \tag{2.3.10}$$

we get that:

$$f'(\xi) = \partial_\xi f(\xi) = \frac{u_\xi}{u_v}. \tag{2.3.11}$$

We can expand u_ξ and u_v by coordinate transforms to get the following:

$$u_\xi = [\partial_\xi x^r \cdot \partial_r \bar{\phi} + \partial_\xi x^t \partial_t \bar{\phi}]/\sqrt{X} = \frac{V+U}{\xi^2(1-\xi)}, \tag{2.3.12}$$

and

$$u_v = [\partial_v x^r \cdot \partial_r \bar{\phi} + \partial_r x^t \partial_t \bar{\phi}]/\sqrt{X} = U, \tag{2.3.13}$$

so:

$$f'(\xi) = \frac{u_\xi}{u_v} = \frac{-V-U}{\xi^2(\xi-1)U}. \tag{2.3.14}$$

The new time coordinate is now explicitly defined in terms of U V and ξ, allowing the metric to be written in the form of:

$$\mathrm{d}s^2 = (1-\xi)\,\mathrm{d}\tau^2 - \frac{2V}{\xi^2 U}\,\mathrm{d}\tau\,\mathrm{d}\xi - \frac{1}{\xi^4 U^2}\,\mathrm{d}\xi^2 - \frac{1}{\xi^2}\,\mathrm{d}\Omega^2\,. \tag{2.3.15}$$

It is now a somewhat long, but straightforward process to incorporate these ansatz for the perturbed field (2.3.1). We focus on the first spherical harmonic (2.3.5) and collect terms of quadratic order in $\chi(\xi)$ to get

$$S = 2\pi M^2 \alpha \int \mathrm{d}\tau \mathrm{d}\xi \left(A(\xi)(\chi'')^2 + B(\xi)(\chi')^2 + C(\xi)\chi^2 \right). \tag{2.3.16}$$

The coefficients read:

$$A(\xi) = U^4V^2\xi^4 - c_\chi^2 U^6 \xi^4 \tag{2.3.17}$$

$$\begin{aligned} B(\xi) = \;& 2\xi^2U^2V^2 - \xi^4U^4VV'' - \xi^4U^5U'' - 4\xi^4U^3V^2U'' - 2\xi^4U^2V^2U'^2 \\ & - 4\xi^3U^4VV' - 8\xi^3U^3V^2U' - 4\xi^4U^3VU'V' - 2\xi^2U^4V^2 \\ & - c_\chi^2(4\xi^2U^4 - 3\xi^4U^4VV'' - 3\xi^4U^5U'' - 6\xi^4U^4U'^2 - 12\xi^3U^5U' + 6\xi^2U^4V^2) \end{aligned} \tag{2.3.18}$$

$$\begin{aligned} C(\xi) = \;& 2[-\xi^2U^3U'' - \xi^2UV^2U'' - \xi^2U^2U'^2 - 2\xi UV^2U' - 2\xi^2UVU'V' \\ & + c_\chi^2(\xi^2U^2VV'' + \xi^2U^3U'' + 3\xi^2U^2U'^2 + 10\xi U^3U' + 2U^4 - 2U^2V^2 - 2U^2)] \end{aligned} \tag{2.3.19}$$

The action (2.3.16) gives equations of motion for the perturbation as:

$$(A\chi'')'' - (B\chi')' + C\chi = 0. \tag{2.3.20}$$

2.3.3 Singular Behaviour in Equations of Motion

With an equation of motion derived for χ it is pertinent to determine whether it is well behaved, and if not, to identify where special care needs to be given. We will consider points where the equations of motions become singular, and find the conditions that need to be placed on χ so that the physical observable of the theory u^μ is non-singular.

From (2.3.17) we see that $A(\xi)$ vanishes at $\xi = 0, \xi_c, \xi_\star$. If $B(\xi)$ and $C(\xi)$ had zeroes of order larger than $A(\xi)$ then there would be no issue. However, a Taylor series analysis of these terms at these points leads to the orders of zeroes of various functions shown in Table.1.

$(\xi - \xi_0)^{\alpha_X}$	α_A	α_B	α_C
$\xi_0 = 0$	4	2	1
$\xi_0 = \xi_c$	1	0	0
$\xi_0 = \xi_\star$	4	2	1

Table 1: The power of the zeroes for each coefficient at each singular point. Here, α_X represents the lowest order power appearing in the expansion of the X coefficient around the point ξ_0. We see that the zeroes of A are always stronger than those of B or C indicating they are true singularities of the equation of motion.

The conclusion is that the points $\xi = 0, \xi_c, \xi_\star$ represent true singularities of the equation (2.3.20). To account for this we will have to consider the form of χ at each of these singular points. For instance at $\xi = 0$ we have already determined that the solution should behave like $\frac{1}{\xi}$ in (2.3.5). At ξ_c and $\xi_\star$ the gradient vector of the perturbation δu^μ should be non-singular.

To find the conditions on the vector we first find the variation of the vector u^μ then insert a series expansion of χ around the singular points and find the minimal power

acceptable for χ so that the vector components do not diverge. We now consider the variation of the foliation leaves in the Eddington-Finkelstein coordinates:

$$\begin{aligned}\delta u^\mu &= \delta\left(\frac{\partial^\mu\phi}{\sqrt{\partial_\lambda\phi\partial^\lambda\phi}}\right)\\ &= \frac{\partial^\mu\delta\phi}{\sqrt{\partial_\lambda\phi\partial^\lambda\phi}} - \partial^\nu\delta\phi\partial_\nu\phi\frac{\partial^\mu\phi}{(\partial_\lambda\phi\partial^\lambda\phi)^{\frac{3}{2}}}\end{aligned} \tag{2.3.21}$$

here we take the perturbation of ϕ to be the scalar field Ξ and group terms of the original u^μ:

$$\delta u^\mu = \frac{\partial^\nu\Xi(\xi,\theta)}{\sqrt{\partial_\lambda\bar{\phi}\partial^\lambda\bar{\phi}}}(\delta^\mu_\nu - \bar{u}_\nu\bar{u}^\mu). \tag{2.3.22}$$

Where overbars indicate they represent the background field solutions. The square root term can be expanded explicitly in Eddington-Finkelstein coordinates using the same trick as (2.3.9) and (2.3.10):

$$\sqrt{\partial_\lambda\bar{\phi}\partial^\lambda\bar{\phi}} = \frac{1}{U}. \tag{2.3.23}$$

Next, we specify for the cases of $\mu = \xi, v, \theta, \varphi$:

$$\begin{aligned}\delta u^\xi &= -U^3\xi^4\partial_\xi\Xi(\xi,\theta) = -U^3\xi^4\partial_\xi\chi(\xi)\cos\theta \\ \delta u_v &= VU^2\xi^2\partial_\xi\Xi(\xi,\theta) = VU^2\xi^2\partial_\xi\chi(\xi)\cos\theta, \\ \delta u_\theta &= U\partial_\theta\Xi(\xi,\theta) = U\partial_\theta\chi(\xi)\cos\theta, \\ \delta u_\phi &= U\partial_\phi\Xi(\xi,\theta) = 0.\end{aligned} \tag{2.3.24}$$

$\chi(\xi - \xi_0)$	Minimal power
$\xi_0 = 0$	ξ^{-1}
$\xi_0 = \xi_c$	$(\xi - \xi_c)^0$
$\xi_0 = \xi_\star$	$(\xi - \xi_\star)^{-1}$

Table 2: Minimal power expansion of perturbed khronon field so that the normalized gradient of the foliation remains non-singular.

Then, we can write the radial component of χ as a Taylor series:

$$\chi(\xi) = (\xi - \xi_0)^q \sum_{k=0}^{\infty} c_k (\xi - \xi_0)^k. \tag{2.3.25}$$

This has a partial derivative with respect to ξ of:

$$\partial_\xi \chi(\xi) = \sum_{k=0}^{\infty} c_k (k+q)(\xi - \xi_0)^{k+q-1} \tag{2.3.26}$$

Let us first consider $\xi_0 = \xi_\star$. If we insert this series expansion of χ into equation (2.3.24) and taking into account that U is proportional to $\xi - \xi_\star$ around $\xi_\star$ we get that around χ near $\xi_\star$ the perturbation χ can diverge at most at order $(\xi - \xi_\star)^{-1}$

At spatial infinity, we only permit powers greater than ξ^{-1} as this corresponds to an order of r which fits with the model of a moving black hole when viewed at infinity:

$$\chi(r) \approx vr\cos\theta \tag{2.3.27}$$

Finally, at $\xi = \xi_c$ the perturbation χ must diverge no faster that $(\xi - \xi_c)^0$.

The results of the minimal allowed power of χ such that the solutions remain finite are summarized in Table.2.

It is also prudent to consider the behaviour of the khronon stress-energy tensor through the regime we are interested in. Particularly we would expect that the stress energy tensor through this regime should be finite down to the universal horizon. If the stress energy tensor was singular at any point then we should also reject any solutions which give this behaviour. This analysis is performed in Appendix.A.1 but does not yield any extra constraints. In fact, we find that once the conditions listed in Table.2 are satisfied, the stress-energy tensor is regular everywhere at $\xi < \xi_\star$ and vanishes at $\xi = \xi_\star$.

2.3.4 Frobenius Analysis

We have just determined the forms of χ that are allowed so that the physical observable of the theory u^μ remains finite. The goal now turns to finding solutions of χ. Still, we will not be able to analytically solve the equations of motions and will need to solve them numerically. However, this requires having boundary conditions. To find the boundary conditions, we will consider the forms of χ via the Frobenius around the points 0, ξ_c, $\xi_\star$. The Frobenius method will provide us with the linearly independent series expansions of χ that satisfy the equations of motion.

We shall see that each expansion point will provide 4 unique solutions as would be expected from a 4th order equation. However, at each point, one solution will be rejected by not having a power incompatible with Table.2. This provides us with three conditions which together with normalization at infinity are sufficient to uniquely fix the solution of the linear fourth-order equation (2.3.20).

Applying general theorems to equation (2.3.20) we see that if $A(\xi)$ has zeroes then the solution may have poles or a branch cut. At every zero of A, $\xi = 0, \xi_c, \xi_\star$, we

substitute the solution in the form of $\chi \propto (\xi - \xi_0)^\lambda$ and expand the equation into Taylor series. Requiring the leading zeroes to vanish provides an equation for λ. We will explicitly show the calculation for $\xi = 0$; the calculations for $\xi = \xi_c,\ \xi = \xi_\star$ are analogous. We take a series expansion of various coefficients in (2.3.20) around $\xi = 0$ and obtain:

$$\begin{aligned} 0 =& \lambda(\lambda-1)(\lambda-2)(\lambda-3)\xi^{\lambda-4} + R_1\lambda(\lambda-1)(\lambda-2)\xi^{\lambda-3} \\ &+(R_2+R_3)\lambda(\lambda-1)\xi^{\lambda-2} + R_4\lambda\xi^{\lambda-1} + R_5\xi^\lambda, \end{aligned}$$

where

$$R_1 = \lim_{\xi\to 0}\frac{2A'}{A}\xi = 8 \tag{2.3.28}$$

$$R_2 = \lim_{\xi\to 0}\frac{A''}{A}\xi^2 = 12 \tag{2.3.29}$$

$$R_3 = \lim_{\xi\to 0}\frac{-B}{A}\xi^2 = -4 \tag{2.3.30}$$

$$R_4 = \lim_{\xi\to 0}\frac{-B'}{A}\xi^3 = -8 \tag{2.3.31}$$

$$R_5 = \lim_{\xi\to 0}\frac{C}{A}\xi^4 = 0. \tag{2.3.32}$$

This gives rise to the set of solutions:

$$\lambda_1^{(0)} = -3, \quad \lambda_2^{(0)} = -1, \quad \lambda_3^{(0)} = 0, \quad \lambda_4^{(0)} = 2. \tag{2.3.33}$$

We reject the solution of $\lambda_4^{(0)}$ as its power is less than the minimum power we found

previously. Next, we can consider the case of $\xi \to \xi_c$ which has solutions of:

$$\lambda_1^{(c)} = 0,\ \lambda_2^{(c)} = 1,\ \lambda_3^{(c)} = 1,\ \lambda_4^{(c)} = 2. \tag{2.3.34}$$

The repeated solution of $\lambda = 1$ would suggest a logarithmic term, however, as the solution needs to be analytic through the sound horizon this term is rejected. Lastly, in the case of $\xi \to \xi_\star$ we get:

$$\lambda_1^{(\star)} = -1,\ \lambda_2^{(\star)} = 0,\ \lambda_3^{(\star)} = -\frac{1}{2} + \sqrt{\frac{2}{\xi_\star^2 U'(\xi_\star)^2} + \frac{1}{4}},\ \lambda_4^{(\star)} = -\frac{1}{2} - \sqrt{\frac{2}{\xi_\star^2 U'(\xi_\star)^2} + \frac{1}{4}}. \tag{2.3.35}$$

In these solutions, we find that $\lambda_4^{(\star)} \leq -1$ so it also must be rejected according to Table.2.

These results represent the starting power of a series expansion which makes up linearly independent solutions at their expansion points. A summary of these powers are in Table.3.

	Soln 1 begins	Soln 2 begins	Soln 3 begins	Soln 4 begins
$\xi = 0$	~~ξ^{-3}~~	ξ^{-1}	1	ξ^2
$\xi = \xi_c$	1	$(\xi - \xi_c)$	$(\xi - \xi_c)^2$	~~$\log(\xi - \xi_c)$~~
$\xi = \xi_\star$	$(\xi - \xi_\star)^{-1}$	1	$(\xi - \xi_\star)^{\lambda_3^{(\star)}}$	~~$(\xi - \xi_\star)^{\lambda_4^{(\star)}}$~~

Table 3: Behaviour of linearly independent solutions of the perturbed khronon field at the 3 singular points of the equation. The powers striked-out are those which are rejected to maintain finite vector components u^μ.

2.3.5 Numerical solutions

Having worked out the behaviour of various solutions of the singular points, we now describe our strategy for solving equation (2.3.20) numerically. At every boundary point, we pick up solutions allowed by the regularity conditions. This gives us 9 linearly independent solutions in total.

We integrate the solutions from the boundary points and match up to 3rd derivatives of the mid-points of the intervals $[0, \xi_c]$ and $[\xi_c, \xi_\star]$. This gives 8 equations for 9 unknowns. We are then left with a single free parameter which we determine by setting the coefficient of the ξ^{-1} solutions at $\xi = 0$ to be 1. This normalization choice corresponds to the choice of black hole velocity.

For numerical integration, we need to step away from the boundary points by a small $\epsilon \approx 10^{-3}$. For this purpose, we find the Taylor series of the solutions at these points up to 3rd order from the Taylor expansion of the equation (2.3.20). We note that since the leading powers of some solutions listed in Table.3 differ by integers, we have to include logarithms in the Taylor expansion. For example at $\xi = 0$ we get:

$$\begin{aligned}\chi^{(0)}_{\alpha_1,\alpha_2,\alpha_3} =& \frac{\alpha_1}{\xi} + \alpha_2 + h_1(\alpha_1,\alpha_2,\alpha_3)\xi + \alpha_3\xi^2 + h_2(\alpha_1,\alpha_2,\alpha_3)\xi^3 + \cdots \\ &+ \log(\xi)(g_1(\alpha_1,\alpha_2,\alpha_3) + g_2(\alpha_1,\alpha_2,\alpha_3)\xi + \cdots).\end{aligned} \tag{2.3.36}$$

Where α_i corresponds to the contribution of each of the 3 linearly independent solutions. It is easy to imagine the form of χ at ξ_c and $\xi_\star$ with the same setup. Using these expansions at each boundary point we solve the differential equation 3 times. Each time we set all but 1 of the primary coefficients to zero and the remaining coefficient

we set to 1. For example, around 0 we would solve with the initial condition that:

$$\begin{aligned}\chi^{(0)}_{1,0,0}(\epsilon) =& \frac{1}{\epsilon} + h_1(1,0,0)\epsilon + h_2(1,0,0)\epsilon^3 + \cdots \\ &+ \log(\epsilon)(g_1(1,0,0) + g_2(1,0,0)\epsilon + \cdots).\end{aligned} \tag{2.3.37}$$

$$\begin{aligned}\chi^{(0)}_{0,1,0} =& 1 + h_1(0,1,0)\epsilon + h_2(0,1,0)\epsilon^3 \cdots \\ &+ \log(\epsilon)(g_1(0,1,0) + g_2(0,1,0)\epsilon).\end{aligned} \tag{2.3.38}$$

$$\begin{aligned}\chi^{(0)}_{0,0,1} =& h_1(0,0,1)\epsilon + \epsilon^2 + h_2(0,0,1)\epsilon^3 \cdots \\ &+ \log(\epsilon)(g_1(0,0,1) + g_2(0,0,1)\epsilon).\end{aligned} \tag{2.3.39}$$

The equations are solved up to the midpoints between the boundaries. The true solution is taken to be a linear combination of these various numerical solutions. To find the contribution of each solution we require that the final solution be continuous up to the 3rd derivative of χ. If the midpoint between $\xi = 0$ and $\xi = \xi_c$ is m_1 then the set of constraints are:

$$\begin{aligned}
\alpha_1\chi^{(0)}_{1,0,0}(m_1) + \alpha_2\chi^{(0)}_{0,1,0}(m_1) + \alpha_3\chi^{(0)}_{0,0,1}(m_1) &= \alpha_4\chi^{(c)}_{1,0,0}(m_1) + \alpha_5\chi^{(c)}_{0,1,0}(m_1) + \alpha_6\chi^{(c)}_{0,0,1}(m_1) \\
\alpha_1\dot{\chi}^{(0)}_{1,0,0}(m_1) + \alpha_2\dot{\chi}^{(0)}_{0,2,0}(m_1) + \alpha_3\dot{\chi}^{(0)}_{0,0,1}(m_1) &= \alpha_4\dot{\chi}^{(c)}_{1,0,0}(m_1) + \alpha_5\dot{\chi}^{(c)}_{0,1,0}(m_1) + \alpha_6\dot{\chi}^{(c)}_{0,0,1}(m_1) \\
\alpha_1\ddot{\chi}^{(0)}_{1,0,0}(m_1) + \alpha_2\ddot{\chi}^{(0)}_{0,1,0}(m_1) + \alpha_3\ddot{\chi}^{(0)}_{0,0,1}(m_1) &= \alpha_4\ddot{\chi}^{(c)}_{1,0,0}(m_1) + \alpha_5\ddot{\chi}^{(c)}_{0,1,0}(m_1) + \alpha_6\ddot{\chi}^{(c)}_{0,0,1}(m_1) \\
\alpha_1\dddot{\chi}^{(0)}_{1,0,0}(m_1) + \alpha_2\dddot{\chi}^{(0)}_{0,1,0}(m_1) + \alpha_3\dddot{\chi}^{(0)}_{0,0,1}(m_1) &= \alpha_4\dddot{\chi}^{(c)}_{1,0,0}(m_1) + \alpha_5\dddot{\chi}^{(c)}_{0,1,0}(m_1) + \alpha_6\dddot{\chi}^{(c)}_{0,0,1}(m_1)
\end{aligned} \tag{2.3.40}$$

and similarly, if the middle point between ξ_c and $\xi_\star$ is labeled m_2 then we get 4 more equations of the form:

$$\begin{aligned}
\alpha_7\chi^{(\star)}_{1,0,0}(m_2) + \alpha_8\chi^{(\star)}_{0,1,0}(m_2) + \alpha_9\chi^{(\star)}_{0,0,1}(m_2) &= \alpha_4\chi^{(c)}_{1,0,0}(m_2) + \alpha_5\chi^{(c)}_{0,1,0}(m_2) + \alpha_6\chi^{(c)}_{0,0,1}(m_2) \\
\alpha_7\dot{\chi}^{(\star)}_{1,0,0}(m_2) + \alpha_8\dot{\chi}^{(\star)}_{0,1,0}(m_2) + \alpha_9\dot{\chi}^{(\star)}_{0,0,1}(m_2) &= \alpha_4\dot{\chi}^{(c)}_{1,0,0}(m_2) + \alpha_5\dot{\chi}^{(c)}_{0,1,0}(m_2) + \alpha_6\dot{\chi}^{(c)}_{0,0,1}(m_2) \\
\alpha_7\ddot{\chi}^{(\star)}_{1,0,0}(m_2) + \alpha_8\ddot{\chi}^{(\star)}_{0,1,0}(m_2) + \alpha_9\ddot{\chi}^{(\star)}_{0,0,1}(m_3) &= \alpha_4\ddot{\chi}^{(c)}_{1,0,0}(m_2) + \alpha_5\ddot{\chi}^{(c)}_{0,1,0}(m_2) + \alpha_6\ddot{\chi}^{(c)}_{0,0,1}(m_2) \\
\alpha_7\dddot{\chi}^{(\star)}_{1,0,0}(m_2) + \alpha_8\dddot{\chi}^{(\star)}_{0,1,0}(m_2) + \alpha_9\dddot{\chi}^{(\star)}_{0,0,1}(m_2) &= \alpha_4\dddot{\chi}^{(c)}_{1,0,0}(m_2) + \alpha_5\dddot{\chi}^{(c)}_{0,1,0}(m_2) + \alpha_6\dddot{\chi}^{(c)}_{0,0,1}(m_2)
\end{aligned} \tag{2.3.41}$$

These 8 equations will reduce the 9 free parameters $(\alpha_1, \cdots, \alpha_9)$ to a single free parameter. This final parameter is constrained by normalizing all of the solutions to having the same velocity at spatial infinity, which corresponds to normalizing $\alpha_1 = 1$ as this corresponds to the spatial asymptotic (2.3.5).

This summarizes the bulk of the procedure in solving solutions to χ, what follows will be some subtleties that are encountered when numerically solving and the steps taken to avoid numerical errors.

The first issue was that despite choosing only the solutions we wanted when starting the shooting method, as numerical errors add up when moving towards the middle points m_1 and m_2 the solution can begin to diverge in an undesirable way. To account for this, a new variable was introduced:

$$\tilde{\chi} = \chi(\xi - \xi_\star)\xi, \tag{2.3.42}$$

so that $\tilde{\chi}$ would not be divergent at the boundaries. This requires modifying the differential equation and redefining the coefficients A, B, and C so that they absorb

the factors of $(\xi - \xi_\star)$ and ξ. Then, after these solutions are solved we convert back to the regular expression for χ.

Secondly, note that $B(\xi)$ appears in in the action (2.3.20) as $B'(\xi)$, which already contains order of $U^{(3)}$. As we will need to take a Taylor series at an ϵ away for the boundary conditions in χ we will need at least 1 more order in derivative, i.e. $U^{(4)}$. However, when numerically solving the background solutions at the boundary only the third-order derivative is calculated, so the fourth-order derivative at boundaries may be inaccurate or discontinuous as they are calculated from discrete values. In Appendix.B (Figure.7) up to 4th order in U derivatives are displayed to assure the reader that the extra derivative is well defined and is behaving in a smooth and continuous manner.

Lastly, to save on computation time the functions $A,\ B,\ C$ are evaluated and interpolated on a grid of points and used as a value look-up function when solving the differential equation. Again, to show that these functions are behaving properly some solutions to $A,\ B,\ C$ are in Appendix.B (Figure.9) are shown.

2.3.6 Numerical Results

With the technical details out of the way, we are now able to appreciate the resulting solutions of χ which are displayed in Figure.4. We notice that the trend of the lines is smooth and well-behaved. Secondly, recall that although the values of χ are divergent the values coordinates of u^μ are not. In fact, we desired that χ would diverge at spatial infinity like $1/\xi$ which we can see in the figure. As well, we can see that the divergence at $\xi_\star$ becomes suppressed for larger values of c_χ.

From χ the perturbations on the aether field can also be calculated and are shown

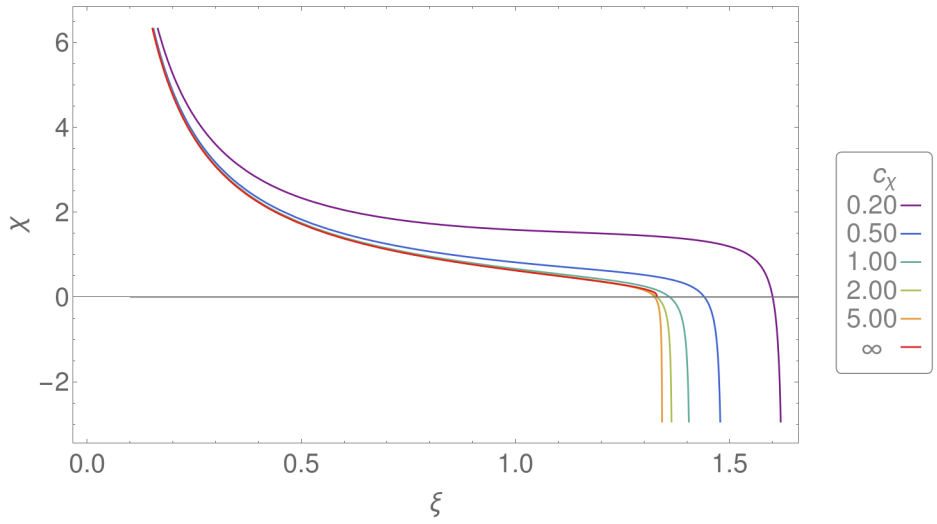

Figure 4: Perturbed field solutions
Solutions of χ for different values of c_χ.

in Figure.5; at spatial infinity, δu^r is growing linearly and δu_v goes to zero. This matches with the intuition developed earlier that the observer at spatial infinity would see the aether field tilted in the radial direction of the black hole. There is also a point where the perturbation of the aether is maximized for both the v and θ components.

Lastly, we note that there is uncertainty about the continuation of the solutions inside of the universal horizon. As the solutions at the universal horizon are non-integer powers. In fact, this behaviour was predicted by [3]. Perhaps it is the case that the solution must be solved internally and matched by boundary conditions at the universal horizon.

2.3.7 Limiting Case of Infinite Khronon Sound Speed

It is instructive to consider the limit $c_\chi = \infty$. As we will see in this case the differential equation for χ greatly simplifies. Comparing the solution in this limit with our general

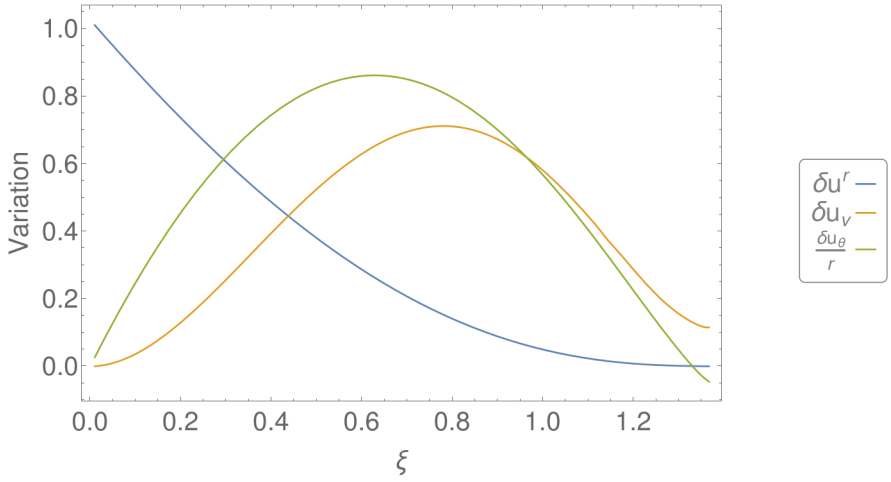

Figure 5: An example of the Aether components perturbation for the solution of $c_\chi = 2$, $\theta = \pi/8$. To make the scales comparable δu^r was scaled by a factor of 1.5, δu_v by a factor of 10, and δu_θ by a factor of 5.

numerical solutions allows us to cross-check our results.

Reading off of (2.2.2) it is easy to show that in the limit of the khronon sound speed going to infinity the equations of motion take the form of:

$$\nabla_\lambda \left(\frac{P^\lambda_\nu}{\sqrt{X}} \nabla^\nu \nabla_\mu u^\mu \right) = 0, \tag{2.3.43}$$

where P^λ_ν is a projection operator:

$$P^\lambda_\nu = \delta^\lambda_\nu - u^\lambda u_\nu. \tag{2.3.44}$$

The left two most operators look like a Laplacian projected on the foliation surfaces:

$$\tilde{\Delta} = \nabla_\lambda \frac{P^\lambda_\nu}{\sqrt{X}} \nabla^\nu, \tag{2.3.45}$$

acting on a scalar:

$$Y = \nabla_\mu u^\mu. \tag{2.3.46}$$

Therefore, we can re-write the equations of motion as:

$$\tilde{\Delta} Y = 0. \tag{2.3.47}$$

It is natural to assume that $\tilde{\Delta}$, like the normal flat-space Laplacian, does not have any zero modes. Then the previous equation implies that $Y = 0$:

$$\nabla_\mu u^\mu = 0. \tag{2.3.48}$$

This can be solved for the unperturbed aether field to get a solution of:

$$U = \sqrt{1 - \xi + \frac{27}{256}\xi^4}. \tag{2.3.49}$$

By perturbing equation (2.3.48) we get a 2nd order differential equation for the perturbed field χ:

$$\left(-\xi^4 + \xi^5 - \frac{27}{256}\xi^8\right)\chi''(\xi) + \left(\frac{3}{2}\xi^4 - \frac{81}{128}\xi^7\right)\chi'(\xi) + 2\xi^2\chi = 0. \tag{2.3.50}$$

We again apply the Frobenius analysis to equation (2.3.50) and obtain a power-law relationship displayed in Table.4. Now notice that in the limit $c_\chi = \infty$ we see that $\xi_c \to \xi_\star$ and the two singularities merge. Thus, we only get 2 boundary points each with an order of 2. As earlier, since all of these roots are integer steps apart we must also include logarithmic terms in case the solutions are degenerate. We find that the

$c_\chi \to \infty$	Soln 1 begins	Soln 2 begins
$\xi = 0$	ξ^{-1}	ξ^2
$\xi = \xi_\star$	~~$(\xi - \xi_\star)^{-1-\sqrt{2}}$~~	$(\xi - \xi_\star)^{-1+\sqrt{2}}$

Table 4: Linearly independent solutions of the perturbed khronon field at the 2 singular points of the equation. The power striked-out are those which are rejected to maintain finite vector components.

logarithmic term persists for both boundaries. Next, an identical matching procedure is completed as before, however, now we only have 3 independent solutions. Matching is still done at the midpoint boundary giving 2 constraints and the final parameter is determined by normalization at a boundary condition. The limiting solution with $c_\chi \to \infty$ is easily included as we can normalize with the same condition as the general solutions.

The solution with $c_\chi = \infty$ is shown in Figure.4 as the red line. We have checked that it indeed represents the limit of solutions with finite c_χ as the parameter increases.

2.4 Sensitivities

Now that we have a set of solutions to the khronon field for a moving black hole we would like to find their observational signatures. To this end we turn to "*sensitivities*." These describe how the mass of a point object depends on its velocity with respect to the preferred frame. We now develop the point particle view of the black hole and determine how the sensitivity parameter matches solutions we previously found. The action for a point particle may be written as:

$$S_{\rm pp} = -\int \mathrm{d}\tau\, m(u_\mu \mathrm{v}^\mu), \tag{2.4.1}$$

where:

$$m = m_0(1 + \sigma(1 - u^\mu \mathrm{v}^\mu)). \tag{2.4.2}$$

Here, σ describes the dependence of the mass on its velocity. Notice that in the case where σ is zero, we obtain the classical description of a point particle.

In the point mass picture we assume that the khronon field is sourced by a point mass very far away in its rest frame, then find perturbations of the khronon field to leading order in coupling parameters:

$$\phi = t + |\mathrm{v}||x|\cos(\theta) + \delta\phi. \tag{2.4.3}$$

We will work with our original Lagrangian for the khronon field to derive the equations of motion. However, we must now include a term sourced by the Ricci tensor which was previously set to 0 when we were working the Schwarzschild metric (2.1.11). Now we get a non-zero contribution localized on the point mass. Additionally, we must consider the Lagrangian terms sourced by the sensitivity parameter.

These additions to the action give it the form of:

$$\begin{aligned} S_\phi = -M^2 \int \mathrm{d}^4x\, \sqrt{-g} \left(\frac{\alpha}{4} u_{\mu\nu} u^{\mu\nu} + \frac{\beta + \lambda}{2} (\boldsymbol{\nabla}_\mu u^\mu)^2 - \frac{1}{2} \beta R_{\mu\nu} u^\mu u^\nu \right) \\ - \int \mathrm{d}\tau\, m_0(1 + \sigma(1 - \mathrm{v}^\mu u^\mu)) \end{aligned}$$

Within this action, we identify 3 separate Lagrangians:

$$\mathcal{L}_{\text{orig}} = -\sqrt{-g}M^2\left(\alpha\frac{1}{4}u_{\mu\nu}u^{\mu\nu} + \frac{\beta+\lambda}{2}(\nabla_\mu u^\mu)^2\right), \tag{2.4.4}$$

$$\mathcal{L}_{\text{ricci}} = \sqrt{-g}\frac{M^2}{2}\beta R_{\mu\nu}u^\mu u^\nu, \tag{2.4.5}$$

$$\mathcal{L}_{\text{sens}} = -m\sigma\delta(x)(1 - \mathrm{v}\cdot u), \tag{2.4.6}$$

In our case the point mass is in its own rest frame where the aether is tilted and so $\mathrm{v}\cdot u$ is just:

$$\mathrm{v}\cdot u = u_0 = \sqrt{1-u_i^2} \approx \left(1 - \frac{u_i^2}{2}\right) \tag{2.4.7}$$

$\mathcal{L}_{\text{orig}}$ and $\mathcal{L}_{\text{ricci}}$ need to be perturbed up to second-order, however since σ is already small we only expand $\mathcal{L}_{\text{sens}}$ up to first order. These perturbation terms still containing power of $\delta\phi$ appears as:

$$\begin{aligned}\delta\mathcal{L}^{(2)}_{\text{orig}} = -\frac{M^2}{2}\Big[&-\alpha\mathrm{v}^k\partial_k h_{00}\Delta\delta\phi + (\beta+\lambda)\Big((\Delta\delta\phi)^2 + 2\mathrm{v}^k\partial_k h_{00}\Delta\delta\phi \\ &- \mathrm{v}^k\partial_k h_{ii}\Delta\delta\phi + 2\mathrm{v}^k\partial_i h_{ki}\Delta\delta\phi\Big)\Big]\end{aligned} \tag{2.4.8}$$

$$\delta\mathcal{L}^{(2)}_{\text{ricci}} = \frac{M^2}{2}\beta\left[-\mathrm{v}^k\partial_k h_{jj}\Delta\delta\phi + \mathrm{v}^k\partial_k\partial_i\partial_j h_{ij}\delta\phi\right] \tag{2.4.9}$$

$$\delta\mathcal{L}^{(1)}_{\text{sens}} = -m\sigma\delta(x)\mathrm{v}^i\partial_i\delta\phi \tag{2.4.10}$$

If we take the equations of motion from just $\delta\mathcal{L}^{(2)}_{\text{orig}}$ and $\delta\mathcal{L}^{(2)}_{\text{ricci}}$ we get

$$\Delta^2\delta\phi(x_i) = \left(\frac{\alpha-\lambda-3\beta}{\beta+\lambda}\right)\mathrm{v}^k\partial_k\Delta\phi_{\text{newt}} \tag{2.4.11}$$

where $\phi_{\rm newt} = -\frac{2m}{M^2 r}$ is the Newtonian potential which appears in the metric as:

$$h_{00} = 2\phi_{\rm newt}, \quad h_{ij} = 2\delta_{ij}\phi_{\rm newt}. \tag{2.4.12}$$

The addition of sensitivity appears in the equations of motion as:

$$\Delta^2\delta\phi(x_i) = \left(\frac{\alpha - \lambda - 3\beta}{\beta + \lambda}\right) \mathrm{v}^k \partial_k \Delta\phi_{\rm newt} - \frac{m\sigma}{M^2(\beta+\lambda)} \mathrm{v}^k \partial_k \delta(x). \tag{2.4.13}$$

We use the relationship for the inverse Laplacian acting on a delta function and express the Newtonian potential in terms of radius:

$$\Delta^{-1}\delta(x) = -\frac{1}{4\pi}\frac{1}{r}, \quad \phi_{\rm newt} = -\frac{Gm}{r}, \quad G = \frac{1}{8\pi M_p^2}, \tag{2.4.14}$$

So that the equation for the perturbed field becomes:

$$\Delta\delta\phi(x_i) = -\frac{Gm}{\beta+\lambda}\left(\alpha - \lambda - 3\beta - 2\sigma\right) v^k \partial_k \left(\frac{1}{r}\right) = A v^k \partial_k \left(\frac{1}{r}\right). \tag{2.4.15}$$

Let:

$$R(x_i) = \frac{1}{r}, \quad \tilde{R}(k_i) = \frac{4\pi}{k^2}, \tag{2.4.16}$$

then take the Fourier transform of both sides:

$$\tilde{\delta}\phi(k_i) = -4\pi i A v^k k_k \frac{1}{k^4} r. \tag{2.4.17}$$

Return to spatial $\delta\phi$ by:

$$\delta\phi(x_i) = -\frac{4\pi i A v^k}{(2\pi)^3} \int \mathrm{d}^3k \, \frac{k_k}{k^4} e^{i\vec{k}\vec{r}}. \tag{2.4.18}$$

The integral evaluates to $i\pi^2 x_k/|x|$, so the expression of $\delta\phi$ becomes:

$$\delta\phi(x_i) = \frac{1}{2}A|v|\cos\theta, \tag{2.4.19}$$

or

$$\delta\phi(x_i) = -\frac{Gm}{2(\beta+\lambda)}\left(\alpha-\lambda-3\beta-2\sigma\right)|v|\cos\theta. \tag{2.4.20}$$

Now, recall we previously worked with the ansatz that the khronon field existed in a Schwarzschild background and perturbed it with the field χ which we solved numerically:

$$\varphi = t + f(r) + \chi(r)|v|\cos(\theta). \tag{2.4.21}$$

Comparing the two expressions for the field at asymptotic infinity (2.4.21)-(2.4.3) we should find that the terms linear with velocity and constant in radius should match. Before we can compare we have to make sure that to the leading order in Gm/r, the metrics are the same. From this condition we identify that the perturbed field needs to be changed into a metric with spherical coordinates, this change results in a constant term added to the radius $|x|_{\text{cart}} \to r|_{\text{schw}} - Gm$ so we can just consider the terms with velocity and a dipole. This gives:

$$-\frac{Gm}{2(\beta+\lambda)}\left(\alpha-\lambda-3\beta-2\sigma\right) + (r-Gm) = \chi(r)_{\text{near } r\to\infty}, \tag{2.4.22}$$

we now enforce the same normalization that was used earlier:

$$r_s = 2Gm = 1. \tag{2.4.23}$$

We saw earlier that the Taylor series of χ around spatial infinity will have the form

of:

$$\chi(r)_{\text{near } r\to\infty} = \frac{1}{\xi} + \chi_0 + \mathcal{O}(\xi) = \delta_0 r + \chi_0 + \mathcal{O}\left(\frac{1}{r}\right). \tag{2.4.24}$$

So the sensitivity is:

$$\sigma = 2\chi_0(\beta+\lambda) + \frac{\alpha+\lambda-\beta}{2}, \tag{2.4.25}$$

Note that up to linear order, this agrees with a separate derivation from [12]. In Figure.6 we list the values of χ_0 for a wide range of numerical solutions plotted against their c_χ value. We see that the fit seems to be converging to:

$$\chi_0 = -\frac{1}{4} + \frac{C}{c_\chi^2}, \tag{2.4.26}$$

for large values of c_χ. The numerical value of $C = 0.0248 \ll 1$. Although the fit was only calculated using χ_0 values from $c_\chi > 1$ we see in Figure.6 that the fit works even for small c_χ. However, as can be seen in Figure.5 for sufficiently small c_χ this relationship does break down. When this is put back into the sensitivity equation we now get:

$$\sigma = \frac{\alpha - 2\beta}{2} + 2\alpha C. \tag{2.4.27}$$

Note, that if the fit is correct, then the parameter λ has dropped from this expression. There are a few takeaways from this final form of the sensitivity parameter. Firstly, the parameters α and β are the most constrained parameters with $|\beta| \leq 10^{-15}$ and $|\alpha| \leq 10^{-7}$ [13]. This means that for most choices of c_χ the sensitivity parameter is tiny. A small sensitivity means that it will be difficult to make observations of the theory by considering mass measurements of moving versus stationary black holes. This could be seen in both a positive and negative light. The optimistic view is that

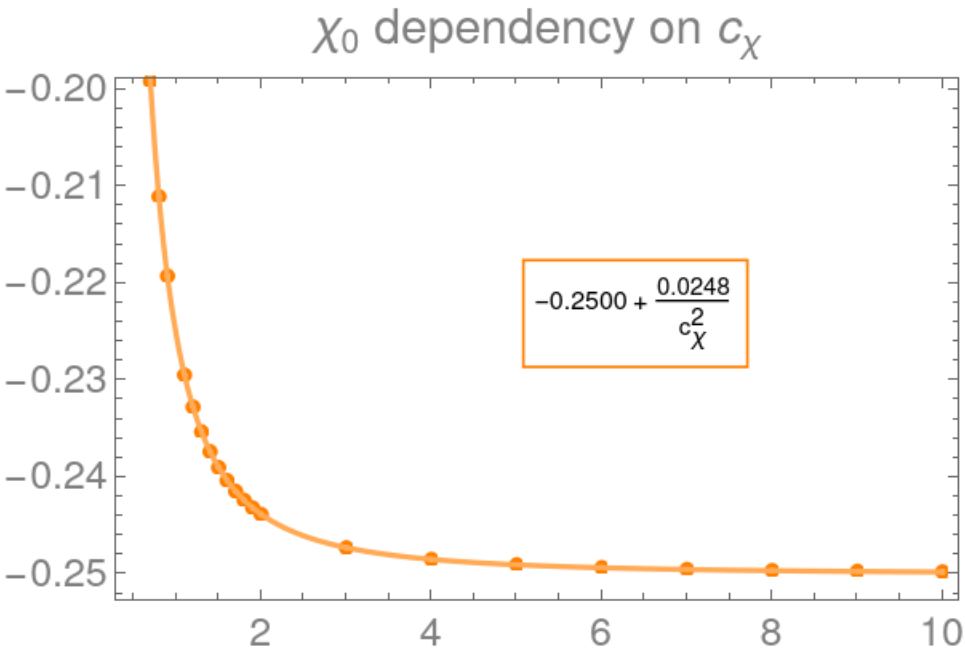

Figure 6: χ_0 parameter fit
χ_0 parameter from numerical solutions plotted against their corresponding c_χ value. The solid orange line depicts the line of best fit for the data.

this is another case where the gravitational regime of the theory matches general relativity while allowing for changes to the quantum theory. The pessimistic view would be that the sensitivity parameter of a black hole will not give a testable prediction of the theory. However, there is one potential benefit to having a small sensitivity parameter: that the sensitivity appears in the calculation of gravitational waves of orbiting binaries. Particularly, it appears as the difference between the sensitivity parameters of the two objects. This would allow a black hole neutron star binary could be a possible test of the theory. Indeed, the neutron star sensitivities are in general non-zero and depend on their compactness [14]. There the black hole sensitivity effectively being zero could maximise the difference. This calculation would make a productive area of future research.

c_χ	χ_0
.1	1.3479
0.5	-0.1511
0.9	-0.2193
1.5	-0.2390
2.0	-0.2438
6.0	-0.2493
10.0	-0.2498

Table 5: Values of χ_0 to show divergence of the coefficient towards small c_χ.

Chapter 3

Results

In this thesis the results of static spherically symmetric black holes in the decoupling limit of Hořava gravity were briefly revisited. In doing so, we verified the results claimed in earlier numerical calculations. These static black holes were used as the basis for a perturbation approach to finding the moving black hole solutions.

Then, a physical picture for a slowly moving black hole were built. The black hole would be given a small velocity v, but instead of sitting in the aether frame, the equations are solved from the black holes rest frame. Then, the boundary conditions were considered at spatial infinity where we expect a small change to flat space-time. These boundary condition were matched with the perturbed khronon field can only have a dipolar effect that at most scales like r.

The equations of motion were then developed giving a 4th order differential equation in terms of the perturbed khronon field and the background field. However, we noticed that the differential equation was singular at various points. Analysis of these singular points gave a set of conditions on the leading order of solutions allowed. Then, using a series expansion at each of the singular points gave 4 possible

solutions, and those that did not obey the conditions were rejected. Ultimately, three solutions were rejected, which provided 3 constraints, leaving a single undefined coefficient. Thus, normalization of these solutions at spatial infinity uniquely defined the solutions.

The full solutions were created for the wide range of the models free parameter c_χ, and from these the perturbations in the aether vector field were also calculated. From the perturbed khronon solutions a novel technique for developing sensitivity parameters for slowly moving black holes were developed. Sensitivity parameters identify the deviation of a point mass particle due to its velocity compared to classical expectations. The order of this sensitivity parameter is primarily controlled by the parameter α. Within the physical constraints of the theory $|\alpha| \leq 10^{-7}$. Thus, the sensitivity parameters were found to be highly suppressed indicating that the deviations from general relativity would be tiny and black holes would appear very similar to their general relativity equivalents.

It is possible that these result may be useful in black hole neutron star binaries where changes to gravitational wave signals appear as the difference between the sensitivities of orbiting bodies. If the neutron star sensitivity is larger than the black hole sensitivity small black hole sensitivity may maximize this difference

Appendix A

Additional Calculations

A.1 Stress Energy Deviation

It is important to consider as well if the choice of allowed non-analytic solutions near the universal horizon makes the stress-energy tensor singular. This would carry with it significant consequences as the metric back reaction would also be singular, and thus the perturbation expansion would not be properly expanded. To this end first notice the perturbed khronon gradients $u_\mu,\ u^\nu$ were designed so that their behaviour was non-singular, but $\chi(\xi)$ could be singular. However, the inclusion of non-analytic solutions at the universal horizon means that with sufficient derivatives their behaviour could become singular. To make this point clear, consider the problematic term of $\chi \propto A(\xi - \xi_\star)^{\lambda_4} \cos\theta$, and that near the horizon $U \approx (\xi - \xi_\star)$. Then, the

perturbed khronon gradients (2.3.24) can be expressed as:

$$\delta\big(u^{\xi}\big) = -A\cos\theta\xi^4(\xi-\xi_\star)^{\lambda_4+2}, \tag{A.1.1}$$

$$\delta(u_v) = A\cos\theta V\xi^2(\xi-\xi_\star)^{\lambda_4+1}, \tag{A.1.2}$$

$$\delta(u_\theta) = -A\sin\theta(\xi-\xi_\star)^{\lambda_4+1}, \tag{A.1.3}$$

$$\delta(u_\phi) = 0. \tag{A.1.4}$$

As well, as it will make the rest of the calculation easier it is best to also include:

$$\delta(u_\xi) = A\cos\theta U^2\frac{(U+V)}{1-\xi}\partial_\xi\chi(\xi,\theta) = A\cos\theta\frac{(U+V)}{1-\xi}(\xi-\xi_\star)^{\lambda_4+1}. \tag{A.1.5}$$

Additionally, $\lambda_4 \in [0,1]$ so we need to be concerned when we see 2 spatial derivatives acting on $u_v,\ u_\theta, u_\xi$. For inspecting the stress-energy tensor we follow the notation used in [12]:

$$J^\rho{}_\mu \equiv \lambda(\nabla_\sigma u^\sigma)\delta^\rho_\mu + \beta\nabla_\mu u^\rho + \alpha a_\mu u^\rho, \tag{A.1.6}$$

$$Æ \equiv \gamma_{\mu\nu}(\nabla_\rho J^{\rho\nu} - \alpha a_\rho\nabla^\nu u^\rho), \tag{A.1.7}$$

$$\gamma_{\mu\nu} \equiv g_{\mu\nu} - u_\mu u_\nu, \tag{A.1.8}$$

$$L_{\rm kh} \equiv \lambda(\nabla_\mu u^\mu)^2 + \beta\nabla_\mu u^\nu\nabla^\nu\nabla_\nu u^\mu + \alpha a_\mu a^\mu, \tag{A.1.9}$$

$$a_\mu \equiv u^\nu\nabla_\nu u^\mu. \tag{A.1.10}$$

So the stress-energy takes the form of:

$$T_{\mu\nu} = \nabla_\rho[J_{(\mu}{}^\rho u_{\nu)} - J^\rho{}_{(\mu}u_{\nu)} - J_{(\mu\nu)}u^\rho] + \alpha a_\mu a_\nu + (u_\sigma\nabla_\rho J^{\rho\sigma} - \alpha a_\rho a^\rho)u_\mu u_\nu + \frac{1}{2}L_{\rm kh}g_{\mu\nu} + 2Æ_{(\mu}u_{\nu)}, \tag{A.1.11}$$

A nice identity to notice is that for our concerns $\nabla_\rho J^\rho_\nu \approx 0$ as the only derivative contraction we care about is when $\rho = \xi$ but that means that we will end up with $^\xi$ which is safe up to 3rd derivatives in ξ, not found in the stress energy. However, from our previous inspections, we also see that we only need to consider terms that contain at least 2 derivatives acting on $u_{v,\theta,\xi}$. Then, for further clarity, we also break down the stress energy into $T^\alpha_{\mu\nu},\ T^\beta_{\mu\nu},\ T^\lambda_{\mu\nu}$ which each contain terms only of their respective coupling constant. We start with the α terms that contain at least a second derivative on u_μ:

$$T^\alpha_{\mu\nu} = -3u_\mu u_\nu u^\xi u^\xi (u^v \partial_\xi \partial_\xi u_v + u^\xi \partial_\xi \partial_\xi u_\xi). \tag{A.1.12}$$

From the definitions of $u^\xi,\ u_\xi,\ u_v,\ u^\xi$ it can be shown that:

$$u^v \partial_\xi \partial_\xi u_v + u^\xi \partial_\xi \partial_\xi u_\xi = 0. \tag{A.1.13}$$

Next, we focus on the terms containing β in the expression:

$$T^\beta_{\mu\nu} = \frac{1}{2} u_\nu \partial_\xi \partial_\xi u_\mu g^{\xi\xi} + \frac{1}{2} u_\mu \partial_\xi \partial_\xi u_\nu g^{\xi\xi} - \frac{1}{2} u^\xi \partial_\xi \partial_\nu u^\sigma g_{\sigma\mu} - \frac{1}{2} u^\xi \partial_\xi \partial_\mu u^\sigma g_{\sigma\nu}, \tag{A.1.14}$$

here we had to solve on a term-by-term basis and find that at worst the terms behave as $\propto U \partial_\xi \partial_\xi u_v$ which goes to zero at the universal horizon and is finite outside of it.

The case for λ should be trivial as $J^{(\lambda)\rho}_\mu = 0$ for our purposes as the trace over $\nabla_\sigma u^\sigma$ which means to have a derivative over ξ would require having u^ξ which is safe up to 3 derivatives. For this reason, it's quick to identify that:

$$T^\lambda_{\mu\nu} = 0. \tag{A.1.15}$$

Since $T^{\alpha}_{\mu\nu},\ T^{\beta}_{\mu\nu},\ T^{\lambda}_{\mu\nu} = 0$ we conclude that the stress energy tensor up to the first order in perturbation is zero at the universal horizon. Thus, we expect no back reaction on the metric at the universal horizon and therefore the perturbation theory should be valid.

A.2 Metric Perturbation corrections

If we take the next order perturbations of (2.4.8) & (2.4.9) and solve for the variational derivative of $h^{(1)}_{\mu\nu} = \delta h_{\mu\nu}$ without considering the sensitivity backreaction on the metric then up to linear order in velocity we get:

$$\Delta h^{(1)}_{00} = \alpha \Delta \phi_{\text{newt}} \tag{A.2.1}$$

$$\Delta h^{(1)}_{i0} = 2(\alpha - 2\beta) v^i \Delta \phi_{\text{newt}} - 2(\alpha - 2\beta) v^j \partial_j \partial_i \phi_{\text{newt}} \tag{A.2.2}$$

$$\Delta h^{(1)}_{ij} = \alpha \delta_{ij} \Delta \phi_{\text{newt}}. \tag{A.2.3}$$

The feedback of the sensitivity can not play into $h^{(2)}_{00}$ or $h^{(2)}_{ij}$ as they appear at to low of a power of v. However, we do see a minimization of $h^{(2)}_{i0}$ components.

$$\Delta h^{(1)}_{00} = \alpha \Delta \phi_{\text{newt}} \tag{A.2.4}$$

$$\Delta h^{(1)}_{k0} = 8\alpha\epsilon v^k \Delta \phi_{\text{newt}} + 8\alpha\epsilon v^j \partial_j \partial_k \phi_{\text{newt}} \tag{A.2.5}$$

$$\Delta h^{(1)}_{ij} = \alpha \delta_{ij} \Delta \phi_{\text{newt}}. \tag{A.2.6}$$

This means that as a whole the next order correction to the metric is of order α suppressed.

Appendix B

Additional Figures

B.1 Additional Figures

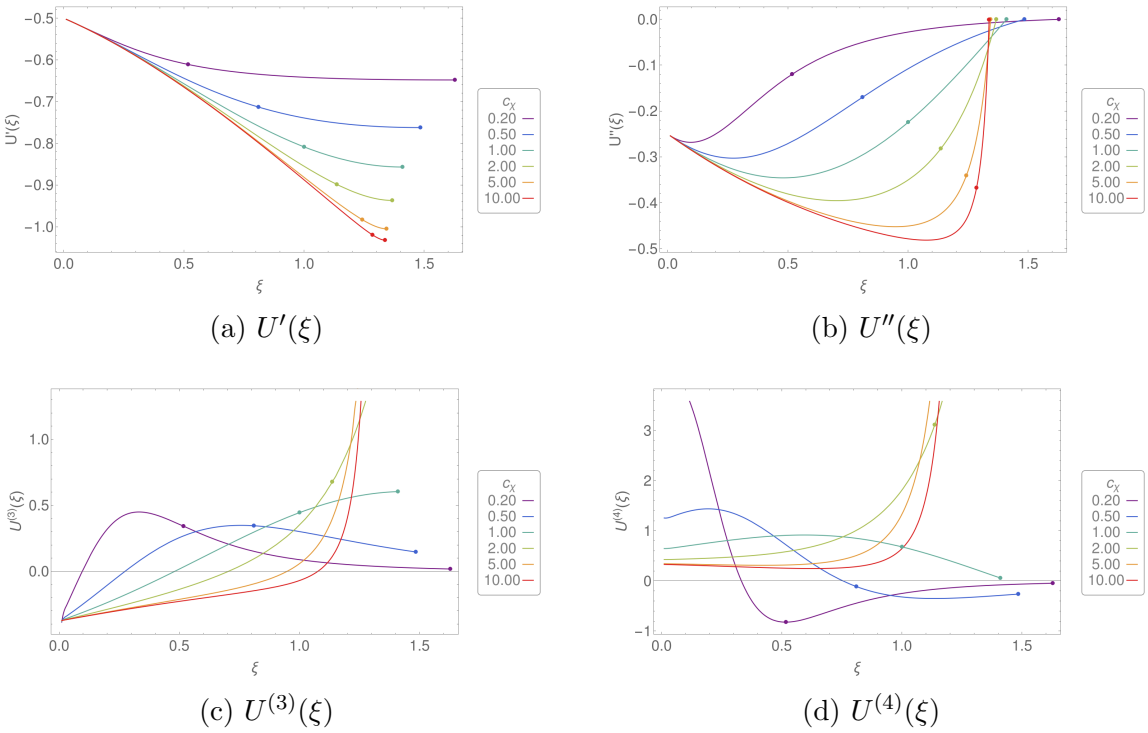

(a) $U'(\xi)$ (b) $U''(\xi)$

(c) $U^{(3)}(\xi)$ (d) $U^{(4)}(\xi)$

Figure 7: Background field high derivatives

High numerical derivatives of the solution obtained by the shooting method. The first coloured dot represents the ξ_c point for each curve and the second coloured dot represents the $\xi_\star$ point for each curve.

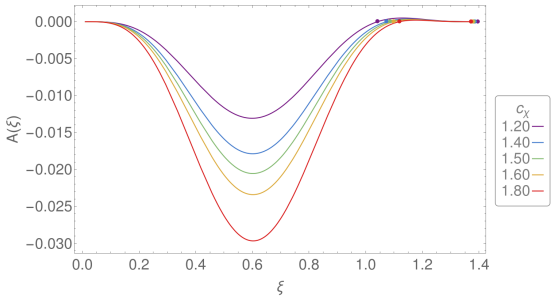

(a) $A(\xi)$

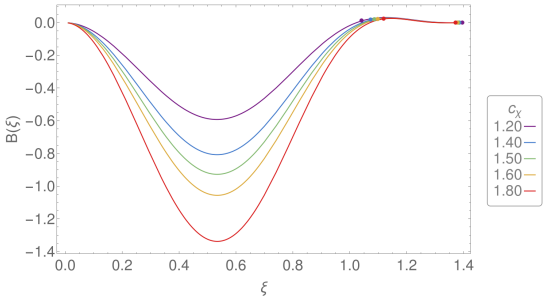

(b) $B(\xi)$

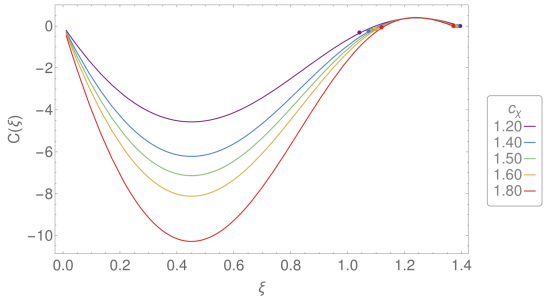

(c) $C(\xi)$

Figure 8: Numerical values of the coefficients A B C for various parameters of c_χ greater than 1. The two ranges were split as it made the curves hard to distinguish otherwise.

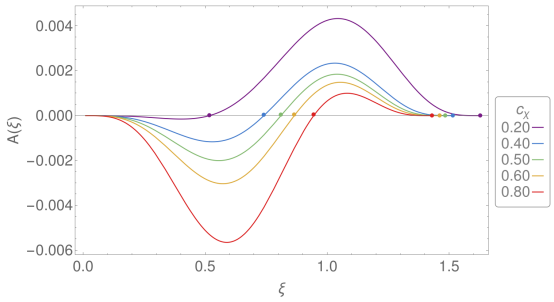

(a) $A(\xi)$

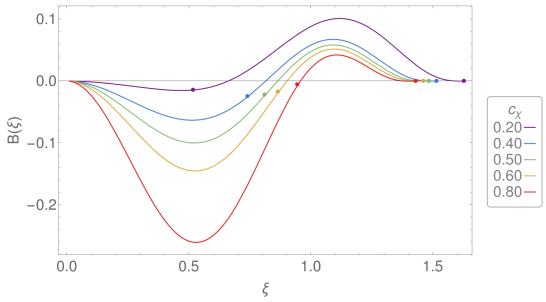

(b) $B(\xi)$

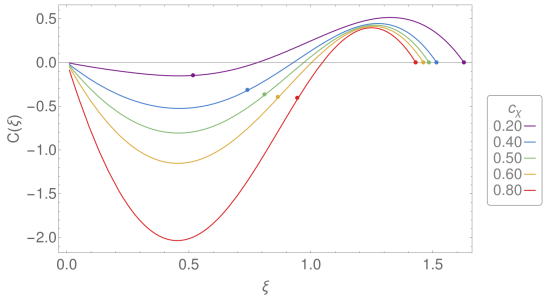

(c) $C(\xi)$

Figure 9: Numerical values of the coefficients A B C for various parameters of c_χ less than 1. By eye, the numerics of A and B may look similar but there is a key distinction in the expansion around ξ_c, note that A begins at $\mathcal{O}(\xi)^1$ whereas B begins at$\mathcal{O}(\xi)^0$.

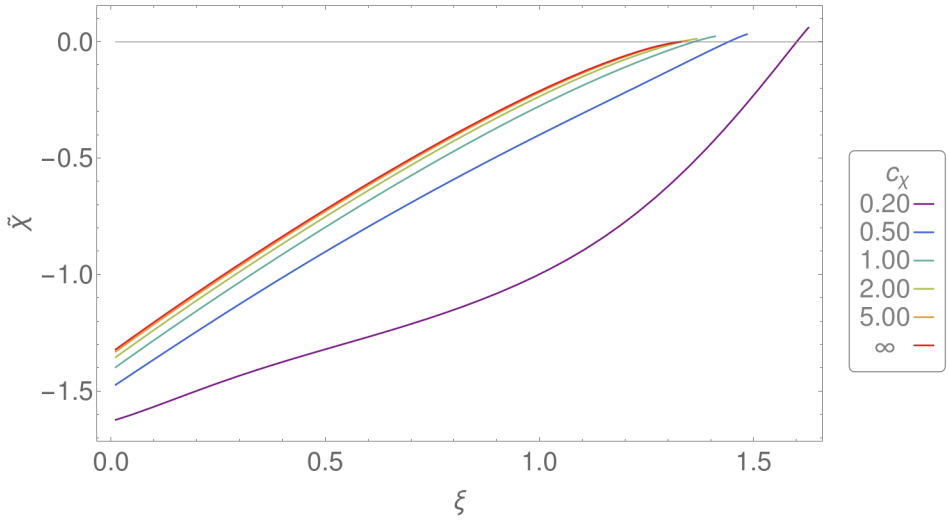

Figure 10: Non divergent perturbed field solutions
Solutions of $\tilde{\chi}$ for different values of c_χ. The coloured data represents the point of ξ_c for the corresponding coloured line.

Bibliography

[1] Petr Hořava. Quantum gravity at a Lifshitz point. *Physical Review D*, 79(8): 084008, April 2009. doi: 10.1103/PhysRevD.79.084008. URL `https://link.aps.org/doi/10.1103/PhysRevD.79.084008`. Publisher: American Physical Society.

[2] Enrico Barausse, Ted Jacobson, and Thomas P. Sotiriou. Black holes in Einstein-aether and Horava-Lifshitz gravity. *Physical Review D*, 83(12):124043, June 2011. ISSN 1550-7998, 1550-2368. doi: 10.1103/PhysRevD.83.124043. URL `http://arxiv.org/abs/1104.2889`. arXiv:1104.2889 [astro-ph, physics:gr-qc, physics:hep-th].

[3] D. Blas and S. Sibiryakov. Horava gravity vs. thermodynamics: the black hole case. *Physical Review D*, 84(12):124043, December 2011. ISSN 1550-7998, 1550-2368. doi: 10.1103/PhysRevD.84.124043. URL `http://arxiv.org/abs/1110.2195`. arXiv:1110.2195 [gr-qc, physics:hep-th].

[4] Enrico Barausse and Thomas P. Sotiriou. Slowly rotating black holes in Horava-Lifshitz gravity. *Physical Review D*, 87(8):087504, April 2013. ISSN 1550-7998, 1550-2368. doi: 10.1103/PhysRevD.87.087504. URL `http://arxiv.org/abs/1212.1334`. arXiv:1212.1334 [gr-qc, physics:hep-th].

[5] D. M. Eardley. Observable effects of a scalar gravitational field in a binary pulsar. *The Astrophysical Journal*, 196:L59–L62, March 1975. ISSN 0004-637X. doi: 10.1086/181744. URL `https://ui.adsabs.harvard.edu/abs/1975ApJ...196L..59E`. ADS Bibcode: 1975ApJ...196L..59E.

[6] Brendan Z. Foster. Radiation Damping in Einstein-Aether Theory. *Physical Review D*, 75(12):129904, June 2007. ISSN 1550-7998, 1550-2368. doi: 10.1103/PhysRevD.75.129904. URL `http://arxiv.org/abs/gr-qc/0602004`. arXiv:gr-qc/0602004.

[7] Brendan Z. Foster and Ted Jacobson. Post-Newtonian parameters and constraints on Einstein-aether theory. *Physical Review D*, 73(6):064015, March 2006. ISSN 1550-7998, 1550-2368. doi: 10.1103/PhysRevD.73.064015. URL `http://arxiv.org/abs/gr-qc/0509083`. arXiv:gr-qc/0509083.

[8] Brendan Z. Foster. Strong field effects on binary systems in Einstein-aether theory. *Physical Review D*, 76(8):084033, October 2007. ISSN 1550-7998, 1550-2368. doi: 10.1103/PhysRevD.76.084033. URL `http://arxiv.org/abs/0706.0704`. arXiv:0706.0704 [gr-qc].

[9] Kent Yagi, Diego Blas, Enrico Barausse, and Nicolas Yunes. Constraints on Einstein-\AE ther theory and Horava gravity from binary pulsar observations. *Physical Review D*, 89(8):084067, April 2014. ISSN 1550-7998, 1550-2368. doi: 10.1103/PhysRevD.89.084067. URL `http://arxiv.org/abs/1311.7144`. arXiv:1311.7144 [astro-ph, physics:gr-qc, physics:hep-ph, physics:hep-th].

[10] Michele Maggiore, Chris van den Broeck, Nicola Bartolo, Enis Belgacem, Daniele Bertacca, Marie Anne Bizouard, Marica Branchesi, Sebastien Clesse, Stefano

Foffa, Juan García-Bellido, Stefan Grimm, Jan Harms, Tanja Hinderer, Sabino Matarrese, Cristiano Palomba, Marco Peloso, Angelo Ricciardone, and Mairi Sakellariadou. Science Case for the Einstein Telescope. *Journal of Cosmology and Astroparticle Physics*, 2020(03):050–050, March 2020. ISSN 1475-7516. doi: 10.1088/1475-7516/2020/03/050. URL `http://arxiv.org/abs/1912.02622`. arXiv:1912.02622 [astro-ph, physics:gr-qc].

[11] Pau Amaro-Seoane, Heather Audley, Stanislav Babak, John Baker, Enrico Barausse, Peter Bender, Emanuele Berti, Pierre Binetruy, Michael Born, Daniele Bortoluzzi, Jordan Camp, Chiara Caprini, Vitor Cardoso, Monica Colpi, John Conklin, Neil Cornish, Curt Cutler, Karsten Danzmann, Rita Dolesi, Luigi Ferraioli, Valerio Ferroni, Ewan Fitzsimons, Jonathan Gair, Lluis Gesa Bote, Domenico Giardini, Ferran Gibert, Catia Grimani, Hubert Halloin, Gerhard Heinzel, Thomas Hertog, Martin Hewitson, Kelly Holley-Bockelmann, Daniel Hollington, Mauro Hueller, Henri Inchauspe, Philippe Jetzer, Nikos Karnesis, Christian Killow, Antoine Klein, Bill Klipstein, Natalia Korsakova, Shane L. Larson, Jeffrey Livas, Ivan Lloro, Nary Man, Davor Mance, Joseph Martino, Ignacio Mateos, Kirk McKenzie, Sean T. McWilliams, Cole Miller, Guido Mueller, Germano Nardini, Gijs Nelemans, Miquel Nofrarias, Antoine Petiteau, Paolo Pivato, Eric Plagnol, Ed Porter, Jens Reiche, David Robertson, Norna Robertson, Elena Rossi, Giuliana Russano, Bernard Schutz, Alberto Sesana, David Shoemaker, Jacob Slutsky, Carlos F. Sopuerta, Tim Sumner, Nicola Tamanini, Ira Thorpe, Michael Troebs, Michele Vallisneri, Alberto Vecchio, Daniele Vetrugno, Stefano Vitale, Marta Volonteri, Gudrun Wanner, Harry Ward, Peter Wass, William Weber, John Ziemer, and Peter Zweifel. Laser Interferometer Space Antenna,

February 2017. URL http://arxiv.org/abs/1702.00786. arXiv:1702.00786 [astro-ph].

[12] Oscar Ramos and Enrico Barausse. Constraints on Ho\v{r}ava gravity from binary black hole observations. *Physical Review D*, 99(2):024034, January 2019. ISSN 2470-0010, 2470-0029. doi: 10.1103/PhysRevD.99.024034. URL http://arxiv.org/abs/1811.07786. arXiv:1811.07786 [gr-qc, physics:hep-ph, physics:hep-th].

[13] A. Emir Gümrükç üoğlu, Mehdi Saravani, and Thomas P. Sotiriou. Hořava gravity after GW170817. *Physical Review D*, 97(2), jan 2018. doi: 10.1103/physrevd.97.024032. URL https://doi.org/10.1103%2Fphysrevd.97.024032.

[14] Toral Gupta, Mario Herrero-Valea, Diego Blas, Enrico Barausse, Neil Cornish, Kent Yagi, and Nicolá s Yunes. New binary pulsar constraints on einstein-æther theory after GW170817. *Classical and Quantum Gravity*, 38(19):195003, aug 2021. doi: 10.1088/1361-6382/ac1a69. URL https://doi.org/10.1088%2F1361-6382%2Fac1a69.